Clays and Clay Minerals, Vol. 58, No. 1, 89–96, 2010.

AB INITIO MOLECULAR DYNAMICS STUDY OF Fe-CONTAINING SMECTITES

XIANDONG LIU[1,*], EVERT JAN MEIJER[2,†], XIANCAI LU[1], AND RUCHENG WANG[1]

[1] State Key Laboratory for Mineral Deposit Research, School of Earth Sciences and Engineering, Nanjing University, Nanjing 210093, P.R. China

[2] Van't Hoff Institute for Molecular Sciences and Amsterdam Center for Multiscale Modeling, University of Amsterdam, Nieuwe Achtergracht 166, 1018 WV Amsterdam, The Netherlands

Abstract—In order to identify the influences imposed by Fe substitution, density functional theory-based Car-Parrinello molecular dynamics simulations were employed to study both oxidized and reduced Fe-bearing smectites. The following basic properties were investigated: local structures in the clay layer, hydroxyl orientations, and the vibration dynamics of H and Si. Structural analyses indicated that the average Fe−O bond lengths are ~2.08 Å and 2.02 Å in the reduced and oxidized models, respectively, and the Fe substitutions did not affect the coordination structures of the Al−O and Si−O polyhedra. For hydroxyl orientations, Fe(III) substitution had no obvious influence but Fe(II) forces the coordinated hydroxyls to present a wide-angle distribution. Furthermore, the present work has shown that both substitutions can red-shift the hydroxyl in-plane bending mode. The analyses also revealed that Fe(III) substitution has no effect on the Si−O stretching, while Fe reduction causes a blue-shift of the out-of-plane stretching mode. The results provide quantitative constraints and clues for future research.

Key Words—CPMD, Density Functional Theory, Hydroxyl Orientation, Iron, Smectite, Vibration Dynamics.

INTRODUCTION

Iron-bearing smectites are of great interest in terms of both basic research and industrial applications (Stucki, 2006). These ubiquitous phyllosilicates form an important pool of Fe in natural ecosystems and have many connections with other inorganic (*e.g.* oxides and carbonates) and organic phases such as bacteria (Alimova *et al*., 2009; Murad and Fischer, 1988). Due to susceptibility to reduction and oxidation reactions, Fe-smectites participate in many reactions and processes, and therefore play active and important roles in the geochemical cycle of Fe (Murad and Fischer, 1988). In industry, smectites are used widely in civil engineering, in the synthesis of composite materials, and in oil exploration. Because of the reduction capability, Fe-bearing smectites are also used in degrading organic pollutants and reducing heavy-metal cations (Cervini-Silva *et al*., 2000; Favre *et al.*, 2006; Jaisi *et al*., 2008a, 2008b; Stucki, 2006; Peretyazhko *et al*., 2008).

Many experimental works have been conducted to study the properties of Fe-smectites and, in particular, the effects of Fe oxidation states. Reduction by Fe is widely acknowledged to alter many properties, such as cation exchange and fixation capacity, specific surface area, layer stacking order, swelling capacity, and surface acidity (Stucki *et al*., 2002; Stucki, 2006). Reliable physical mechanisms for these findings have been difficult to establish, however. In fact, to better understand these issues, some fundamental questions must be answered: (1) How do Fe substitutions (Fe(III) and Fe(II)) affect the crystal structures of smectites? The EXAFS (Extended X-ray Absorption Fine Structure) technique can provide atomic-level structural information, but unequivocal interpretation of EXAFS data is still very difficult (Denecke, 2006). (2) How do the substitutions affect hydroxyl orientation? This is very important for many properties of smectites such as adsorptive properties, and at present is nearly impossible to measure directly. (3) How do the substitutions influence the vibration dynamics of smectites? Techniques such as infrared (IR) and Raman spectroscopy are commonly used in clay sciences, but sometimes the band assignments are questionable and distinguishing the contribution of a single ion species is very difficult (Balan *et al*., 2001; Blanchard *et al*., 2008; Gates, 2008). In addition, smectites are usually fine-grained, poorly crystallized, and always coexist with other minerals, which also increase the problems with data collection in experimental measurements.

Ab initio simulations have been employed on phyllosilicate systems and have proven to be effective for complementing experiments and formulating hypotheses (*e.g.* Cygan and Kubicki, 2001; Kubicki and Bleam, 2003; Larentzos *et al*., 2007; Boulet *et al*., 2006). Only a few studies have focused on Fe-containing phyllosilicates, however. The fundamental questions presented above are rarely investigated and are, therefore, poorly documented.

* E-mail address of corresponding author:
xiandongliu@gmail.com
† e.j.meijer@uva.nl
DOI: 10.1346/CCMN.2010.0580109

Hernandez-Laguna *et al*. (2006), for example, considered the influence of Fe(III) substitution on the total energies of phyllosilicates; Teppen *et al*. (2002) optimized the structure of trichloroethene-intercalated nontronite (an end-member of Fe-smectites in which almost all octahedral metals are Fe); and Rosso and Ilton (2003) focused on electron transfer in Fe-containing micas. The present work aimed to understand those questions with quantum molecular dynamics simulation (Car and Parrinello, 1985). Density functional theory-based molecular dynamics simulations were performed to study both the reduced and oxidized Fe-smectites at finite temperature. The structural and vibrational properties were derived from the trajectories to investigate the effects of Fe substitutions. By comparing the reduced and oxidized systems, the influences of Fe oxidation states were discussed in detail.

METHODOLOGY

The models

The smectite model was derived from the report of Viani *et al*. (2002). The simulated system (Figure 1) consisted of two unit cells ($2a \times b \times c$) with the crystallographic parameters: a = 5.18 Å, b = 8.98 Å, c = 10 Å, $\alpha = \beta = \gamma = 90°$. The unit-cell formula is $Si_8[Al_{3.5}Fe_{0.5}]O_{20}(OH)_4$ where one Al atom is replaced by an Fe in the octahedral sheet. With a single Fe atom, the magnetic ordering can be ignored. Some previous simulation works showed that this system size can properly reproduce the crystal properties of phyllosilicates (*e.g.* Churakov, 2006).

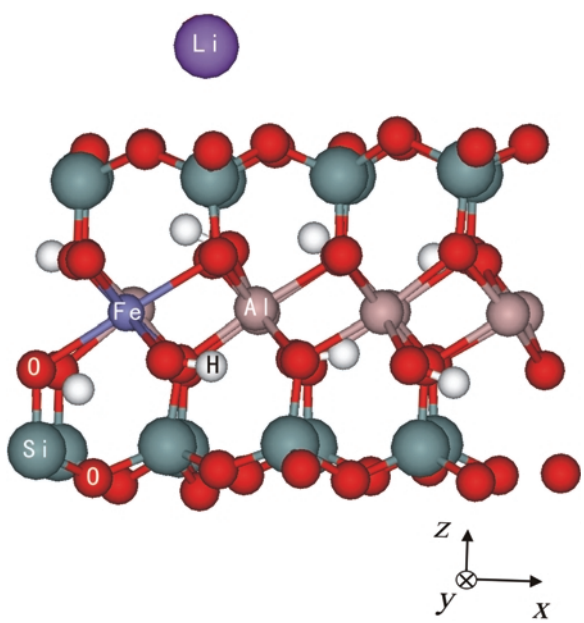

Figure 1. Snapshot of the reduced model.

In the oxidized system, the clay layer is neutral and the interlayer interaction is mainly van der Waals' interaction, so the c-axis length has no obvious influence on the coordination structure in the layer (Churakov, 2006). In the reduced form, the c-axis length is consistent with the experimental measurement of Li-smectite (Calvet, 1973). In this case, a Li^+ cation was inserted in the interlayer space to compensate the negative charge of the clay layer. The cation can be above either the substituted (AlOHFe) or the non-substituted (AlOHAl) six-member ring. In the present study the former is considered and has a slightly lower energy. During the simulation, the interlayer cation always hovered above the six-member ring and did not escape. Smectites generally contain some water molecules in the interlayer spaces, which may have some effect on the vibration dynamics of the substrate (Larentzos *et al*., 2007). No interlayer water molecules were included in the present work in order to exclude the possible additional influences.

Simulation details

The electronic structure was calculated in the framework of density functional theory. The exchange-correlation was described by the Becke-Lee-Yang-Parr (BLYP) function, which adopts the local density approximation augmented with the generalized gradient approximation for the exchange part proposed by Becke (1988) and for the correlation part by Lee *et al.* (1988). The BLYP function has been used to simulate the phyllosilicate systems and produces the bond lengths agreeing with the Perdew-Burke-Ernzerhof functional results and experiments (Churakov, 2006; Liu *et al*., 2008). The BLYP has been shown to describe H-bonding interactions accurately, *e.g.* it gives the best results in liquid water (Sprik *et al*., 1996). The Trouiller-Martins norm-conserving pseudopotentials (Troullier and Martins, 1991) were used to describe the interaction of the valence electrons and the core states, and the Kleinman-Bylander scheme (Kleinman and Bylander, 1982) was applied. The kinetic energy cutoff up to 90 Ry and one K-point in the center of the Brillouin zone ensure a convergence of the bond lengths within 0.02 Å. Iron is in the high-spin state in both oxidized and reduced models.

The molecular dynamics simulations were carried out using the Car and Parrinello approach as implemented in the *CPMD* package (*CPMD version* 3.11) (Car-Parrinello, 1985). The equation of motion was integrated with a time step of 6 a.u. (0.145 fs). In order to use this large time step, the deuterium mass was applied for all hydrogen atoms. The fictitious electronic mass was set at 800 a.u. which maintained the adiabatic conditions. The Nosé-Hoover thermostat was applied to control temperature at 298 K. After equilibration lasting 1 ps, the production number, volume, temperature-constant molecular dynamics runs were performed for 2.2 ps for both systems.

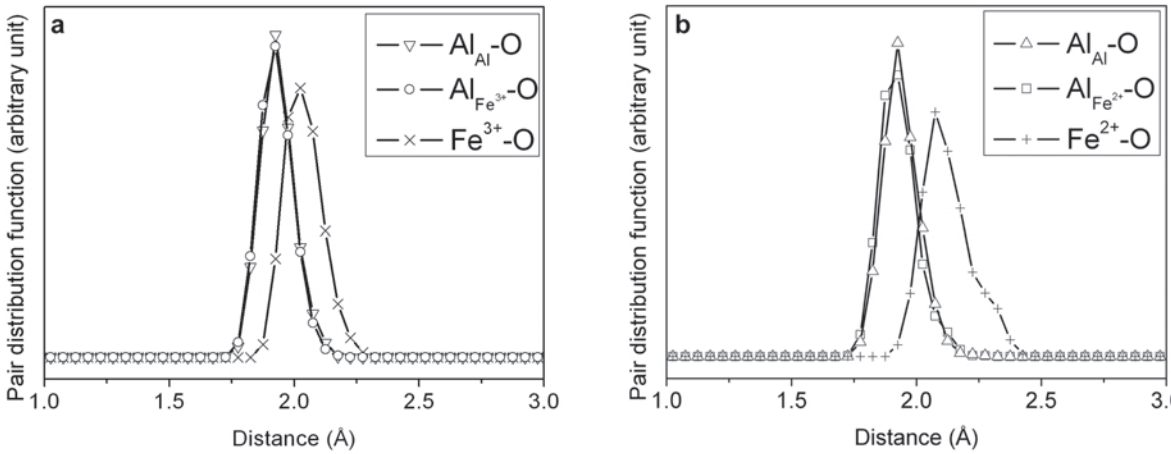

Figure 2. Al−O and Fe−O pair distribution functions in the octahedral sheet of the (a) oxidized and (b) reduced models.

RESULTS AND DISCUSSION

Structures of the clay layer

The pair distribution function of Fe(III)−O (Figure 2a) exhibits a narrow distribution with an average of ~2.02 Å; Fe(II)−O (Figure 2b) presents a slightly wider distribution and shows the peak value at ~2.08 Å. The results are consistent with a previous experimental study (Manceau *et al.*, 2000) in which the bond lengths of Fe(III)−O and Fe(II)−O of nontronite were found to be ~2.01 Å and ~2.10 Å, respectively, by EXAFS analyses. In Figure 2, Al_{Fe} denotes the Al atom connecting with Fe and Al_{Al} refers to the remaining Al atoms. The four Al−O curves are almost the same, ranging from ~1.7 to 2.1 Å in length and are centered at ~1.92 Å, which agrees well with previous reports on systems without Fe substitution (Sainz-Diaz *et al.*, 2002; Refson *et al*., 2003; Larentzos *et al*., 2007).

Si_{Fe} in Figure 3 denotes the Si atom connecting with the Fe atom *via* a bridging oxygen atom, and Si_{Al} indicates those connecting with Al through bridging oxygen. The four Si−O profiles comprise very similar sharp peaks ranging from 1.5 to 1.7 Å and centered at ~1.62 Å. This result is consistent with the previous experiments and quantum simulations (Sainz-Diaz *et al*., 2002; Refson *et al*., 2003; Larentzos *et al*., 2007). The results above suggest that neither Fe(III) nor Fe(II) substitution influences the local structures of the neighboring octahedra and tetrahedra.

Orientations of hydroxyls

The hydroxyl orientation is characterized by the angle between the OH vector and the (100) direction, as depicted in Figure 4. H_{Fe} refers to the H from the hydroxyls coordinating with the Fe atom and H_{Al} denotes the other H atoms. Because one Fe atom is in the model, the total number of H atoms is given by 2 H_{Fe} and 6 H_{Al}. In the oxidized smectite (Figure 4a), both curves represent similar distributions of the OH vector ranging from ~0 to 60º and greatest at ~15−20º. This

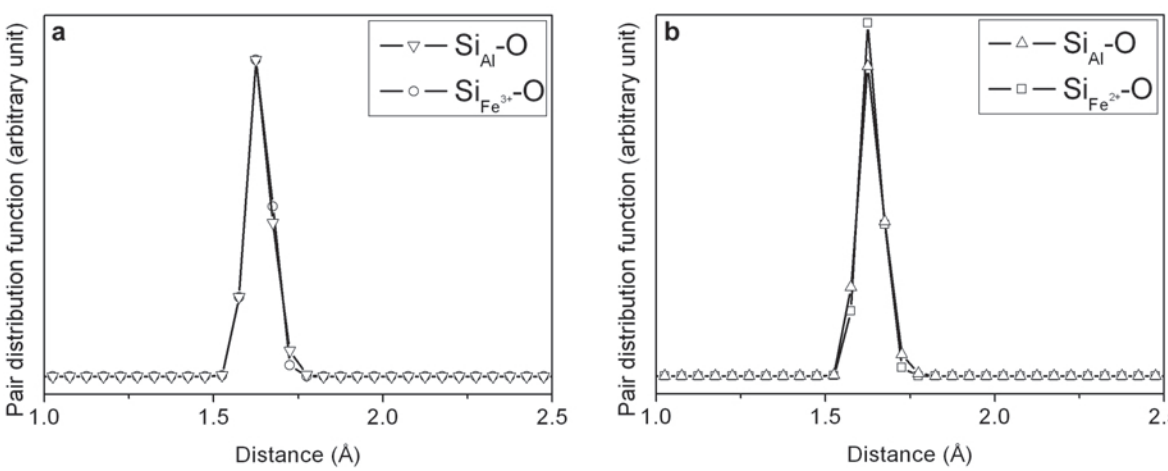

Figure 3. Si−O pair distribution functions in the tetrahedral sheets of the (a) oxidized and (b) reduced models.

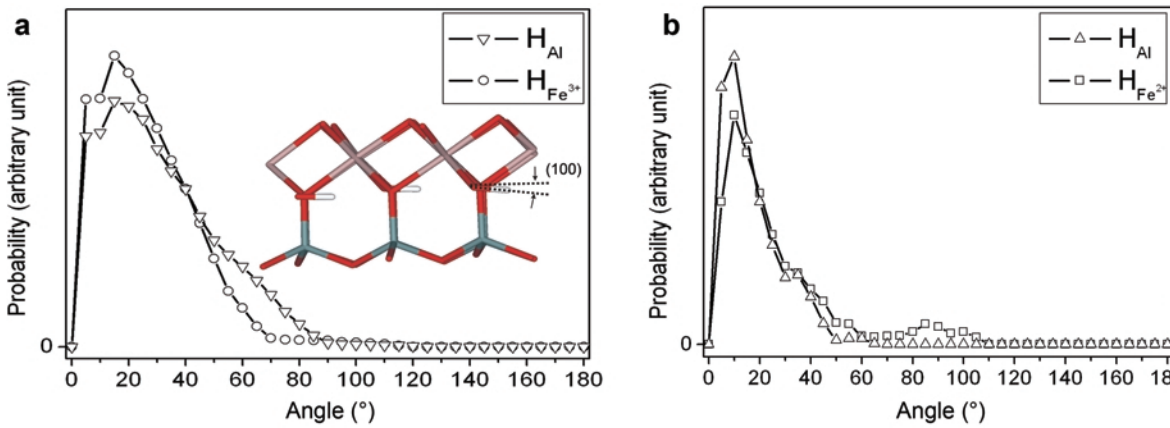

Figure 4. Distributions of hydroxyl orientations in the (a) oxidized and (b) reduced models.

distribution is consistent with the previous *ab initio* molecular dynamics simulations of pyrophyllites (Larentzos *et al*., 2007) and also matches previous static density functional theory (DFT) calculations (Bridgeman *et al*., 1996; Stackhouse *et al*., 2001; Refson *et al*., 2003; Sainz-Diaz *et al*., 2004). In the reduced model, both curves show distributions ranging from ~0 to 40º and $H_{Fe(II)}$ shows another prominent maximum at ~90º (Figure 4b).

Density profiles of hydroxyl hydrogen (Figure 5), in which the middle plane of the clay layer was taken as the origin, revealed very similar distributions for the $H_{Fe(III)}$ and the two H_{Al} , ranging from ~0.5 to 2 Å away from the middle plane (Figure 5a). Remarkably, the $H_{Fe(II)}$ curve exhibited a greater distribution extending to 3 Å (Figure 5b), which is consistent with the distributions reported in Figure 4b.

As noted in the past (Larentzos *et al*., 2007), the hydroxyls point toward the apical oxygen to maximize the electrostatic interaction, leading to a low-angle distribution. The Fe reduction causes the clay layer to be negatively charged and such octahedral substitution is well recognized as being able to make all framework oxygens more negative; therefore, this may be responsible for the narrower low-angle distribution in the reduced model. On the other hand, the Fe−O interaction is weakened after reduction because the Fe−O distance increases, which can impose a greater mobility on the hydroxyl. All of these factors can contribute to the high-angle orientation distribution of the $OH_{Fe(II)}$. The half-width of the clay layer is ~3.3 Å, so when the $OH_{Fe(II)}$ orients to the large-angle region, it is very close to the surface. Structural hydroxyls can significantly affect the interfacial properties, so the special orientation probably contributes to some unique properties of Fe-bearing smectites.

Vibration dynamics

To characterize the vibration dynamics, vibration density of states (VDOS) were calculated from a Fourier

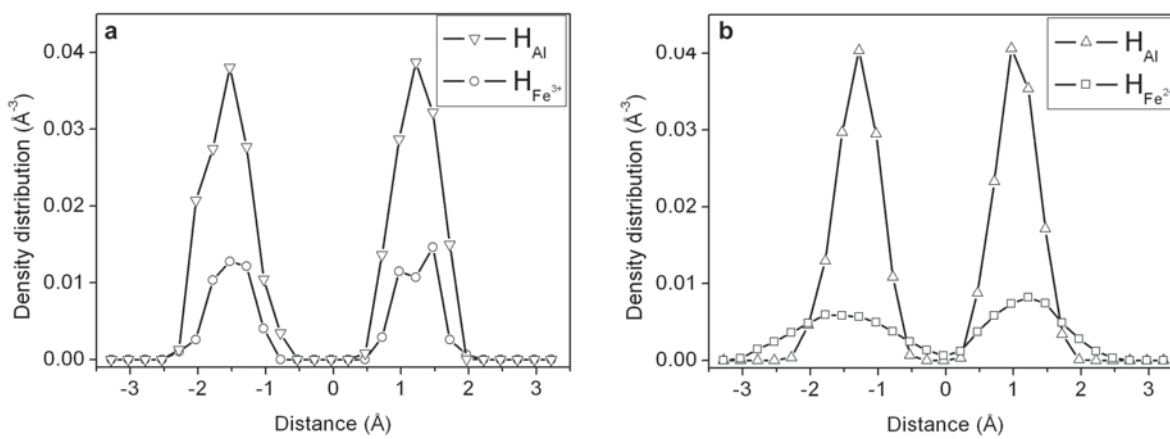

Figure 5. Density distributions of hydroxyl hydrogen in the (a) oxidized and (b) reduced models. The calculations were done $\rho(z) = \langle N(z-\Delta z, z+\Delta z/2)\rangle/(\Delta z \times S)$, where $\langle N(z-\Delta z, z+\Delta z/2)\rangle$ is the averaged atom number occurring in the interval of $(z-\Delta z, z+\Delta z/2)$ and S is the basal surface area.

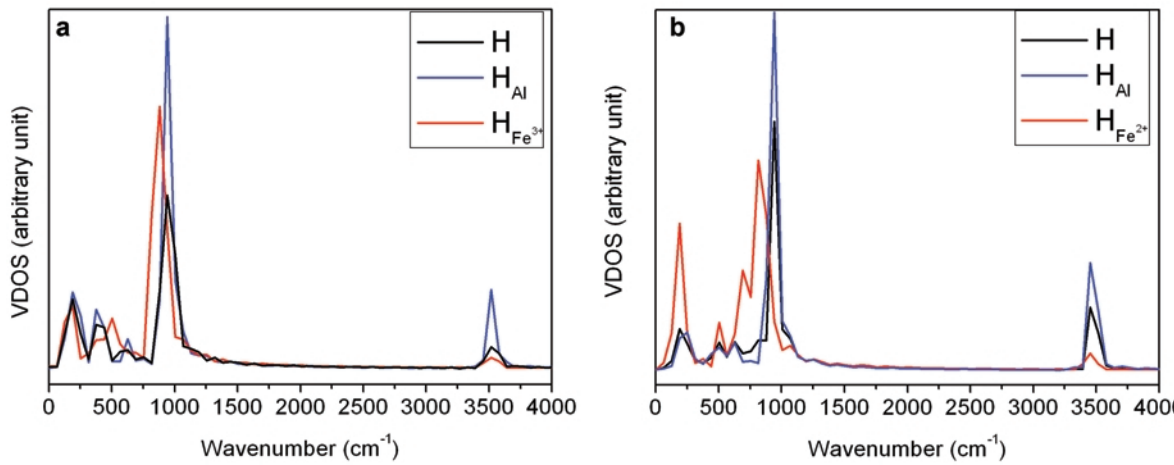

Figure 6. VDOS of hydrogen in the (a) oxidized and (b) reduced models.

transform of the atomic velocity auto-correlation functions (VACF) (Allen and Tildesley, 1987). Such a method was used in simulation analyses of minerals (*e.g.* Boek and Sprik, 2003; Wang *et al*., 2003; Larentzos *et al*., 2007). Generally, the peaks of VDOS indicate some vibration modes which could be either IR or Raman active. Hence, the peak positions can be compared with experimental spectra. The present study focuses on the spectra of H and Si, which are important for experiments (Stucki, 2006). For the calculation of spectra, the atomic velocities were collected every 1.45 fs during the simulations and a correlation time of 0.5 ps was used, giving a resolution of ~20 cm^{-1}.

Because the deuterium mass was used for H in simulations, the calculated VDOS (Figure 6) values were scaled according to $v_H = 1.4 \times v_D$. Three main bands are present in each profile, consistent with other simulation reports (Boek and Sprik, 2003; Sainz-Diaz *et al*., 2004; Larentzos *et al*., 2007). Based on comparisons with previous studies, the band at ~3500 cm^{-1} can be assigned unambiguously to the OH-stretching mode. It also coincides well with the experimental range from 3400 to 3600 cm^{-1} (Farmer, 1974; Bishop *et al*., 2002; Petit, 2006). Botella *et al*. (2004) reported that Fe(III) substitution can shift the stretching to the lower-frequency region, which is not detected on the calculated spectrum. However, the presence of Fe(II) yields a lesser stretching frequency than Fe(III), which is consistent with experiments (Manceau *et al*., 2000; Fialips *et al*., 2002). In both the oxidized and reduced smectites, the spectra of H_{Al} showed the in-plane bending mode of Al_2-OH at ~930 cm^{-1}, which agrees well with experimental measurements (Farmer, 1974; Bishop *et al*., 2002). Red-shifts of the in-plane bending modes can be observed in both H_{Fe} spectra: ~890 cm^{-1} if Fe(III) and 820 cm^{-1} if Fe(II). The reducing trend is consistent with the previous

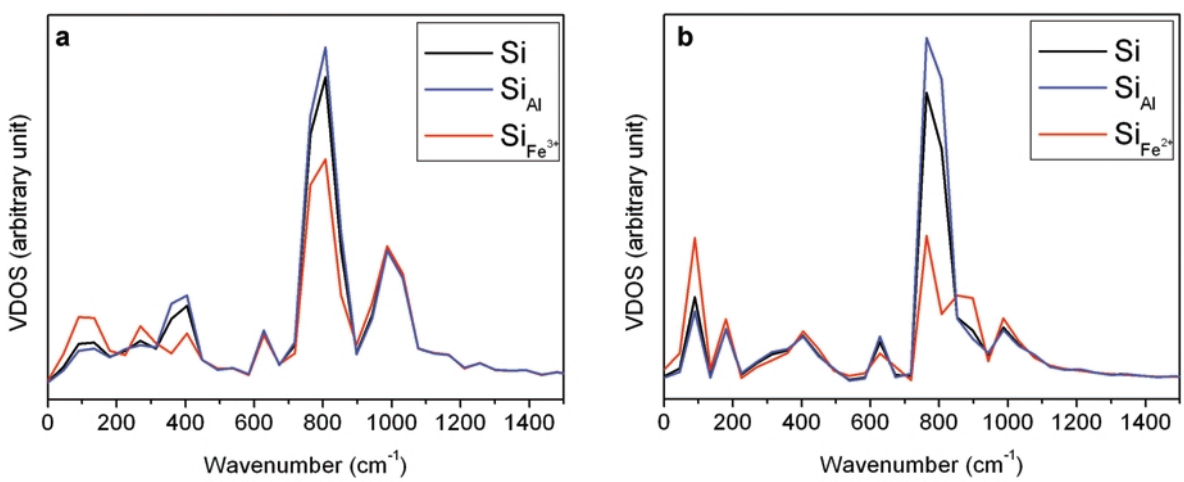

Figure 7. VDOS of silicon in the (a) oxidized and (b) reduced models.

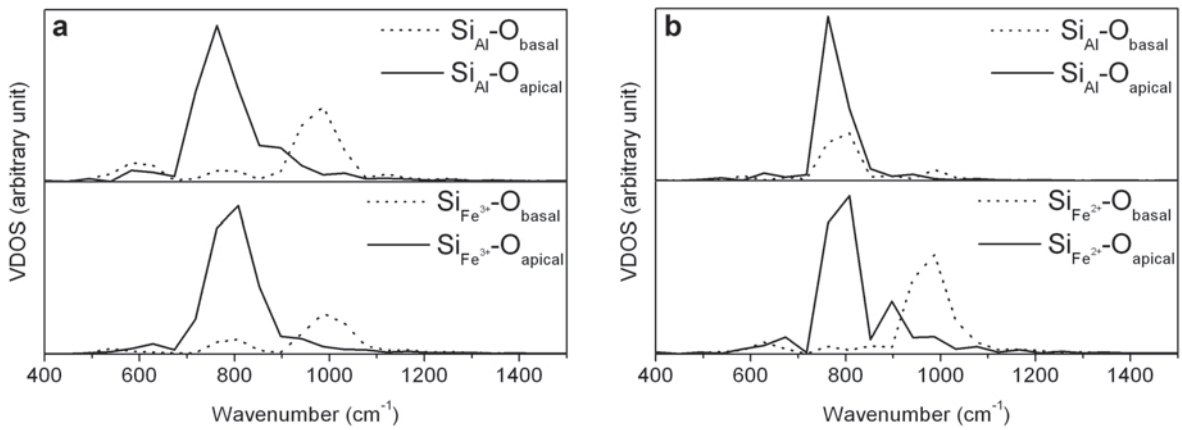

Figure 8. Power spectra of Si−O bonds in the (a) oxidized and (b) reduced models.

calculation (Botella *et al*., 2004) and experiments (Goodman *et al*., 1976). Because one Fe atom is present in each model, *i.e*. only two (AlFe)-OH hydroxyls, the red-shifts have not been reflected in the spectra of all hydrogen (black lines in Figure 6). As for the bands below 700 cm^{-1}, the low-frequency modes such as the out-of-plane bending of OHs and some libration modes are included (Farmer, 1974; Bishop *et al*., 2002).

In the vibrational spectra of modes involving Si (Figure 7), the following domains can be distinguished: ~900−1100 cm^{-1}, 700−900 cm^{-1}, 650 cm^{-1}, and below 400 cm^{-1}. In the spectra of $Si_{Fe(II)}$ (Figure 7b), the 700−900 cm^{-1} domain splits into two peaks.

In order to assign the Si−O stretching modes, the power spectra of Si−O bonds (Figure 8) were calculated by Fourier transforming the auto-correlation functions of Si−O bond lengths (Gaigeot and Sprik, 2003). In one Si−O tetrahedron, the three Si−O_{basal} interactions were very similar, but they were different from the Si−O_{apical} interaction. By comparing Figure 7 with Figure 8, the bands at ~900−1100 cm^{-1}, ~700−900 cm^{-1}, and 650 cm^{-1} are all attributed to the Si−O stretching modes, consistent with previous reports (Bougeard *et al*., 2000). The Si−O_{basal} stretching contributes to all three bands, whereas the Si−O_{apical} stretching contributes mainly to the latter two bands. In Figure 7b, an additional peak at ~900 cm^{-1} can be observed on the Si−O_{apical} spectrum, which corresponds to the peak in the spectrum of $Si_{Fe(II)}$ (Figure 7b).

The analyses above can also be confirmed by the component VDOS. The anisotropic VDOS contributions (XX, YY, and ZZ; Figure 9) are calculated for each Si type using only the relevant **x**, **y**, and **z** projections of the velocity vectors. In the present systems, the **x** and **y** components of velocities are within the plane, parallel to the basal surface, and the **z** component is perpendicular to the basal surface. Therefore, XX and YY reflect the correlations of motions within the plane parallel to the basal surface and ZZ reflects that perpendicular to the basal surface. The Si−O_{basal} vector is almost parallel to the basal plane, so its stretching contribution is mainly on XX and YY. As can be seen in Figure 9, all XX and

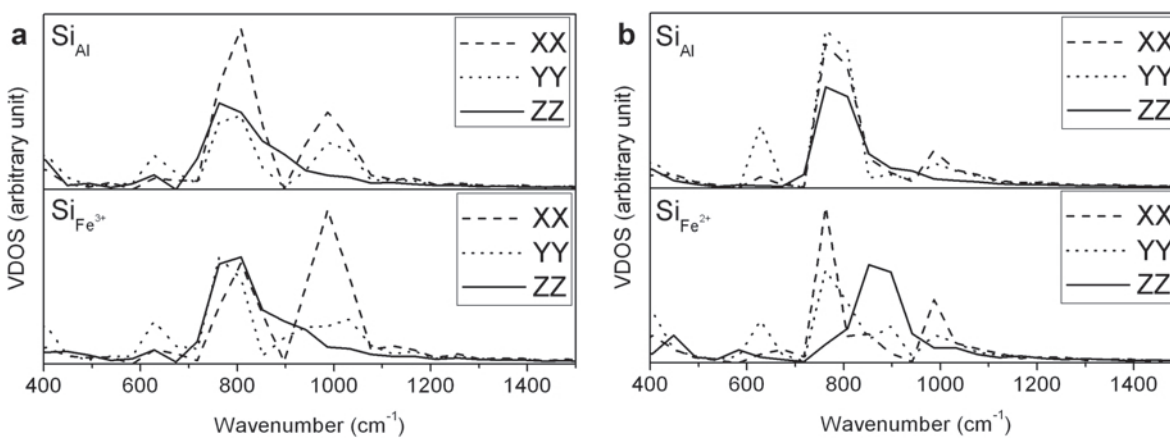

Figure 9. Component VDOS of silicon in the (a) oxidized and (b) reduced models.

YY curves contribute to the bands at 800 cm^{-1} and 1000 cm^{-1}, which thus correspond to the contribution of $Si-O_{basal}$ stretching. Because the $Si-O_{apical}$ vector is approximately perpendicular to the basal surface, its stretching mode contributes mainly to the out-of-plane vibration, *i.e.* on ZZ. The spectra show that the ZZ contribution to the band at 1000 cm^{-1} is trivial. In Figure 9b, the ZZ of $Si_{Fe(II)}$ is shifted to higher frequency, which corresponds to the peak located at ~900 cm^{-1} (Figures 7b, 8b). A previous IR spectroscopy study of Fe-containing smectites (Yan and Stucki, 1999) indicated that Fe reduction can increase the out-of-plane Si−O stretching frequency, which is qualitatively consistent with the finding in the $Si_{Fe(II)}$ spectrum.

SUMMARY

In the present study, the structural and vibrational properties of Fe-bearing smectites were investigated in detail using *ab initio* molecular dynamics. The average Fe−O bond length was found to be ~2.08 Å in the reduced smectite and ~2.02 Å in the oxidized model. Neither substitution imposed significant influence on the coordination structures of the Al−O and Si−O polyhedra. For hydroxyl orientations, Fe(III) substitution had no obvious influence whereas Fe(II) forced the coordinated hydroxyls to present a broader distribution. Both substitutions were found to shift the in-plane bending of hydroxyls downward and the Fe(II) substitution can red-shift the stretching frequencies. The Si−O stretching was not influenced by Fe(III) substitution, but the out-of-plane stretching mode can be shifted upwards by Fe reduction.

ACKNOWLEDGMENTS

X. Liu thanks Bernd Ensing and Weijie Hua for fruitful discussions. The authors thank Dr Bei Liu for a critical reading of the manuscript. They also acknowledge Jiangsu Project Innovation for PhD Candidates (CX07B-049z) and the Scientific Research Foundation of the Graduate School of Nanjing University.

REFERENCES

Alimova, A., Katz, A., Steiner, N., Rudolph, E., Wei, H., Steiner, J. C., and Gottlieb, P. (2009) Bacteria-clay interaction: structural changes in smectite induced during biofilm formation. *Clays and Clay Minerals*, **57**, 205−212.

Allen, M. P. and Tildesley, D. J. (1987) *Computer Simulation of Liquids*. Clarendon Press, Oxford, UK.

Balan, E., Saitta, A.M., Mauri, F., and Calas, G. (2001) First-principles modeling of the infrared spectrum of kaolinite. *American Mineralogist*, **86**, 1321−1330.

Becke, A.D. (1988) Density-functional exchange-energy approximation with correct asymptotic behavior. *Physical Review A*, **38**, 3098−3100.

Bishop, J., Murad, E., and Dyar, M.D. (2002) The influence of octahedral and tetrahedral cation substitution on the structure of smectites and serpentines as observed through infrared spectroscopy. *Clay Minerals*, **37**, 617−628.

Blanchard, M., Lazzeri, M., Mauri, F., and Balan, E. (2008) First-principles calculation of the infrared spectrum of hematite. *American Mineralogist*, **93**, 1019−1027.

Boek, E.S. and Sprik, M. (2003) Ab initio molecular dynamics study of the hydration of a sodium smectite clay. *Journal of Physical Chemistry B*, **107**, 3251−3256.

Botella, V., Timon, V., Escamilla-Roa, E., Hernandez-Languna, A., and Sainz-Diaz, C.I. (2004) Hydrogen bonding and vibrational properties of hydroxy groups in the crystal lattice of dioctahedral clay minerals by means of first principles calculations. *Physics and Chemistry of Minerals*, **31**, 475−486.

Bougeard, D., Smirnov, K.S., and Geidel, E. (2000) Vibrational spectra and structure of kaolinite: A computer simulation study. *Journal of Physical Chemistry B*, **104**, 9210−9217.

Boulet, P., Greenwell, H.C., Stackhouse, S., and Coveney, P.V. (2006) Recent advances in understanding the structure and reactivity of clays using electronic structure calculations. *Journal of Molecular Structure: THERMOCHEM*, **762**, 33−48.

Bridgeman, C.H., Buckingham, A.D., Skipper, N.T., and Payne, M.C. (1996) Ab-initio total energy study of uncharged 2:1 clays and their interaction with water. *Molecular Physics*, **89**, 879−888.

Calvet, R. (1973) Hydratation de la montmorillonite et diffusion des cations compensateurs. I. Saturation par des cations monovalents. *Annales Agronomiques*, **24**, 77−133.

Car, R. and Parrinello, M. (1985) Unified approach for molecular-dynamics and density-functional theory. *Physical Review Letters*, **55**, 2471−2474.

Cervini-Silva J., Wu, J., Stucki, J.W., and Larson, R.A. (2000) Adsorption kinetics of pentachloroethane by iron-bearing smectites. *Clays and Clay Minerals*, **48**, 132−138.

Churakov, S.V. (2006) Ab initio study of sorption on pyrophyllite: structure and acidity of the edge sites. *Journal of Physical Chemistry B*, **110**, 4135−4146.

Cygan, R.T. and Kubicki, J.D. (editors) (2001) *Molecular Modeling Theory: Applications in the Geosciences*. Volume **42**, Reviews in Mineralogy and Geochemistry, Mineralogical Society of America, Chantilly, Virginia, and the Geochemical Society, St. Louis, Missouri.

Denecke, M. (2006) Actinide speciation using X-ray absorption fine structure spectroscopy. *Coordination Chemical Reviews*, **250**, 730−754.

Farmer, V.C. (1974) The layer silicates. Pp. 331−363 in: *The Infrared Spectra of Minerals* (V.C. Farmer, editor). Monograph **4**, Mineralogical Society, London.

Favre, F., Stucki, J.W., and Boivin, P. (2006) Redox properties of structural Fe in ferruginous smectite. A discussion of the standard potential and its environmental implications. *Clays and Clay Minerals*, **54**, 466−472.

Fialips, C.I., Huo, D.F., Yan, L.B., Wu, J., and Stucki, J.W. (2002) Effect of Fe oxidation state on the IR spectra of Garfield nontronite. *American Mineralogist*, **87**, 630−641.

Gaigeot, M.P. and Sprik, M. (2003) Ab initio molecular dynamics computation of the infrared spectrum of aqueous uracil. *Journal of Physical Chemistry B*, **107**, 10344−10358.

Gates, W.P. (2008) Cation mass-valence sum (CM-VS) approach to assigning OH-bending bands in dioctahedral smectites. *Clays and Clay Minerals*, **56**, 10−22.

Goodman, B.A., Russell, J.D., Fraser, A.R., and Woodhams, F.W.D. (1976) Mössbauer and IR spectroscopic study of structure of nontronite. *Clays and Clay Minerals*, **24**, 53−59.

Hernandez-Laguna, A., Escamilla-Roa, E., Timon, V., Dove, M.T., and Sainz-Diaz, C.I. (2006) DFT study of the cation arrangements in the octahedral and tetrahedral sheets of dioctahedral 2:1 phyllosilicates. *Physics and Chemistry of Minerals*, **33**, 655−666.

Jaisi, D.P., Dong, H.L., and Morton, J.P. (2008a) Partitioning of Fe(II) in reduced nontronite (NAu-2) to reactive sites: Reactivity in terms of Tc(VII) reduction. *Clays and Clay Minerals*, **56**, 175–189.

Jaisi, D.P., Ji, S.S., Dong, H.L., Blake, R.E., Eberl, D.D., and Kim, J.W. (2008b) Role of microbial Fe(III) reduction and solution chemistry in aggregation and settling of suspended particles in the Mississippi River delta plain, Louisiana, USA. *Clays and Clay Minerals*, **56**, 416–428.

Kleinman, L. and Bylander, D.M. (1982) Efficacious form for model pseudopotentials. *Physical Review Letters*, **48**, 1425–1428.

Kubicki, J.D. and Bleam, W.F. (2003) *Molecular Modeling of Clays and Mineral Surfaces.* CMS Workshop Lectures volume **12**, The Clay Minerals Society, Aurora, Colorado, USA.

Larentzos, J.P., Greathouse, J.A., and Cygan, R.T. (2007) An ab initio and classical molecular dynamics investigation of the structural and vibrational properties of talc and pyrophyllite. *Journal of Physical Chemistry C*, **111**, 12752–12759.

Lee, C., Yang, W., and Parr, R.G. (1988) Development of the colle-salvetti correlation-energy formula into a functional of the electron-density. *Physical Reviews B*, **37**, 785–789.

Liu, X.D., Lu, X.C., Wang, R.C., Zhou, H.Q., and Xu, S.J. (2008) Surface complexes of acetate on edge surfaces of 2:1 type phyllosilicate: Insights from density functional theory calculation. *Geochimica et Cosmochimica Acta*, **72**, 5896–5907.

Manceau, A., Drits, V.A., Lanson, B., Chateigner, D., Wu, J., Huo, D., Gates, W.P., and Stucki, J.W. (2000) Oxidation-reduction mechanism of iron in dioctahedral smectites: II. Crystal chemistry of reduced Garfield nontronite. *American Mineralogist*, **85**, 153–172.

Murad, E. and Fischer, W.R. (1988) Geobiochemical cycle of iron. Pp. 1–18 in: *Iron in Soils and Clay Minerals* (J.W. Stucki, B.A. Goodman, and U. Schwertmann, editors). D. Reidel, Dordrecht, The Netherlands.

Peretyazhko, T., Zachara, J.M., Heald, S.M., Jeon, B.H., Kukkadapu, R.K., Liu, C., Moore, D., and Resch, C.T. (2008) Heterogeneous reduction of Tc(VII) by Fe(II) at the solid-water interface. *Geochimica et Cosmochimica Acta*, **72**, 1521–1539.

Petit, S. (2006) Fourier transform infrared spectroscopy. Pp. 909–918 in: *Handbook of Clay Science* (F. Bergaya, B.K.G. Theng, and G. Lagaly, editors). Elsevier, Amsterdam.

Refson, K., Park, S.H., and Sposito, G. (2003) Ab initio computational crystallography of 2:1 clay minerals: 1. Pyrophyllite-1Tc. *Journal of Physical Chemistry B*, **107**, 13376–13383.

Rosso, K.M. and Ilton, E.S. (2003) Charge transport in micas: The kinetics of Fe-II/III electron transfer in the octahedral sheet. *Journal of Chemical Physics*, **119**, 9207–9218.

Sainz-Diaz, C.I., Escamilla-Roa, E., and Hernandez-Laguna, A. (2004) Pyrophyllite dehydroxylation process by first principles calculations. *American Mineralogist*, **89**, 1092–1100.

Sainz-Diaz, C.I., Timon, V., Botella, V., Artacho, E., and Hernandez-Laguna, A. (2002) Quantum mechanical calculations of dioctahedral 2:1 phyllosilicates: Effect of octahedral cation distributions in pyrophyllite, illite, and smectite. *American Mineralogist*, **87**, 958–965.

Sprik, M., Hutter, J., and Parrinello, M. (1996) Ab initio molecular dynamics simulation of liquid water: Comparison three gradient-corrected density functionals. *Journal of Chemical Physics*, **105**, 1142–1152.

Stackhouse, S., Coveney, P.V., and Sandre, E. (2001) Plane-wave density functional theoretic study of formation of clay-polymer nanocomposite materials by self-catalyzed in situ intercalative polymerization. *Journal of the American Chemical Society*, **123**, 11764–11774.

Stucki, J.W. (2006) Properties and behavior of iron in clay minerals. Pp. 423–476 in: *Handbook of Clay Science* (F. Bergaya, B.K.G. Theng, and G. Lagaly, editors). Elsevier, Amsterdam.

Stucki, J.W., Lee, K., Zhang, L.Z., and Larson, R.A. (2002) Effects of iron oxidation state on the surface and structural properties of smectites. *Pure and Applied Chemistry*, **74**, 2145–2158.

Teppen, B.J., Yu, C.H., Newton, S.Q., Miller, D.M., and Schafer, L. (2002) Quantum molecular dynamics simulations regarding the dechlorination of trichloro ethene in the interlayer space of the 2:1 clay mineral nontronite. *Journal of Physical Chemistry A*, **106**, 5498–5503.

Troullier, N. and Martins, J.L. (1991) Efficient pseudopotentials for plane-wave calculations. *Physical Reviews B*, **43**, 1993–2006.

Viani, A., Gaultieri, A.F., and Artioli, G. (2002) The nature of disorder in montmorillonite by simulation of X-ray powder patterns. *American Mineralogist*, **87**, 966–975.

Wang, J., Kalinichev, A.G., Amonette, J., and Kirkpatrick, R.J. (2003) Interlayer structure and dynamics of Cl-bearing hydrotalcite: far infrared spectroscopy and molecular dynamics modeling. *American Mineralogist*, **88**, 398–409.

Yan, L. and Stucki, J.W. (1999) Effects of structural Fe oxidation state on the coupling of interlayer water and structural Si-O stretching vibrations in montmorillonite. *Langmuir*, **15**, 4648–4657.

(*Received 11 February 2009; revised 6 October 2009; Ms. 283; A.E. P. Komadel*)